Photofission of actinide nuclei in the quasideuteron and lower part of the Δ energy region

J. C. Sanabria,* B. L. Berman, C. Cetina, P. L. Cole,† and G. Feldman
Center for Nuclear Studies, Department of Physics, The George Washington University, Washington, D.C. 20052

N. R. Kolb, R. E. Pywell, and J. M. Vogt‡
Saskatchewan Accelerator Laboratory, Saskatoon, Saskatchewan, Canada S7N 0W0

V. G. Nedorezov and A. S. Sudov
Institute for Nuclear Research, Russian Academy of Sciences, Moscow 117312, Russia

G. Ya. Kezerashvili§
Budker Institute of Nuclear Physics, Novosibirsk 630090, Russia

(Received 28 May 1999; revised manuscript received 25 October 1999; published 11 February 2000)

The total photofission cross sections for the actinide nuclei ^{232}Th, ^{233}U, ^{235}U, ^{238}U, and ^{237}Np have been measured from 68 to 264 MeV using tagged photons at the Saskatchewan Accelerator Laboratory. The fission fragments were detected using parallel-plate avalanche detectors. The results show that the fission probability for ^{238}U is 20% lower than that for ^{237}Np and 40% higher than that for ^{232}Th. Less significant differences were also found among the individual uranium isotopes. These results contradict the assumption that the fission probability for ^{238}U is approximately equal to unity in this energy range. It has also been observed that the fission probability as a function of energy for all these isotopes is constant, with the exception of that for ^{232}Th, which increases with energy, although it seems to be reaching a saturation value. Comparison between the total photofission cross section for ^{237}Np and the photoabsorption cross sections for lighter nuclei shows a behavior consistent with a broadening of the Δ resonance with increasing atomic mass.

PACS number(s): 25.20.−x, 25.85.Jg, 27.90.+b

I. INTRODUCTION

A. Motivation

The total photofission cross section, in the case of the heavy actinides, has been thought to be a good approximation to the total photoabsorption cross section at photon energies well above the giant dipole resonance region. This allows one to study the effect of the nuclear medium on processes such as baryon resonance formation and propagation within the interior of the nucleus. Specifically, for the case of ^{238}U, experimental measurements and theoretical calculations have suggested that the photofission probability is consistent with unity for photon energies larger than about 40 MeV [1,2]. Comparison of the total photofission cross section per nucleon for the uranium nuclei with the total photoabsorption cross section per nucleon for nuclei from Be to Pb in the Δ-resonance region (from approximately 200 MeV to 450 MeV photon energy) shows a similar shape and strength for these cross sections, indicating that the photoabsorption process can be described by an incoherent total volume absorption mechanism [3]. However, this conclusion is in part based on the assumption that the photofission probability of uranium is close to unity [4]. Even the most recent results using monochromatic photons [5–7] show some discrepancies in the cross sections per nucleon for ^{235}U and ^{238}U and between these isotopes and the so-called ''universal curve'' in the Δ-resonance region.

The most important discrepancy reported previously appears in the results of a measurement of the relative photofission probability of ^{237}Np compared with ^{238}U from 60 MeV to 240 MeV photon energy [8]. In this measurement the photofission probability of ^{237}Np appears to be between 20% and 30% larger than that of ^{238}U, so that the photofission probability for the latter isotope could be at most 0.8. This result has serious implications for the inferred total photoabsorption cross-section strengths in the Δ-resonance region, and needs to be verified.

The lack of direct measurements of the total photoabsorption cross sections for actinide isotopes, together with the discrepancies mentioned above, makes it very important to measure very accurately the absolute and relative photofission cross section for ^{237}Np and several uranium isotopes.

The availability of high-duty-cycle electron accelerators like the ones at Mainz, Saskatchewan Accelerator Laboratory (SAL), and Jefferson Laboratory, together with their photon-tagging facilities, allows one to measure the photofission cross sections for actinide nuclei very accurately over a wide range of photon energies. A simultaneous measurement of these cross sections under identical conditions determines their relative fissilities.

*Present address: Departamento de Física, Universidad de los Andes, A.A. 4976, Bogotá, Colombia.
†Present address: Department of Physics, University of Texas, El Paso, TX 79968.
‡Present address: Hypres Inc., Elmsford, NY 10523.
§Deceased.

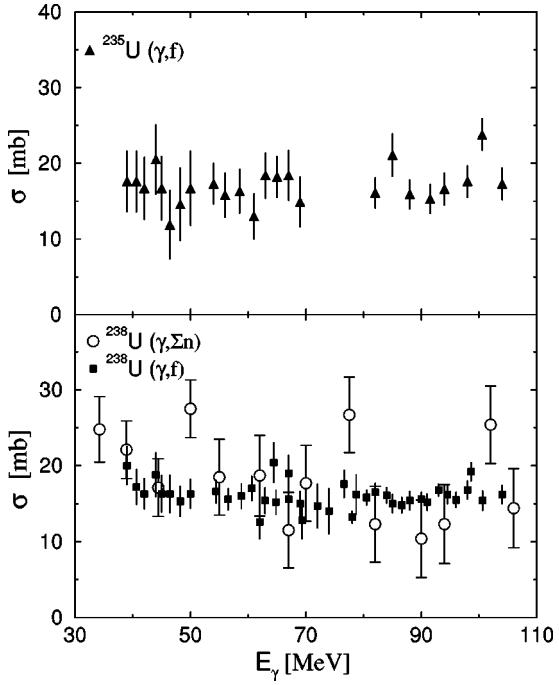

FIG. 1. Photofission cross section for ^{235}U (solid triangles), and ^{238}U (solid squares), compared with the ''total'' photoneutron cross section for ^{238}U (open circles) [1].

The accurate measurement of the total photofission cross sections for ^{232}Th, ^{233}U, ^{235}U, ^{238}U, and ^{237}Np from 68 to 264 MeV at SAL has provided us with explanations for the discrepancies mentioned above.

B. Previous measurements

A careful and comprehensive inspection of the existing data on photoabsorption and photofission for heavy nuclei is necessary in order to determine the level of certainty in the knowledge of the fission probability of actinide nuclei and of the ''universal'' behavior of the photoabsorption cross section per nucleon. The photon energy spectrum can be divided into several regions based on the different absorption mechanisms: the giant dipole resonance, the quasideuteron, the Δ resonance, and the higher resonances.

In the giant dipole resonance region the total photofission cross sections for several actinide nuclei have been measured very accurately using monoenergetic photons from the annihilation in flight of fast positrons [9–12]. The fission probability measured in these experiments in the energy region near 10 MeV varies from 0.1 for the case of ^{232}Th up to about 0.6 for the case of ^{237}Np.

In the quasideuteron region (from approximately 40 MeV photon energy up to the pion threshold), the quality of the data is not as good as in the giant dipole resonance region. In Fig. 1 the total photofission cross sections for ^{235}U and ^{238}U [1] are compared with the only data on total photoabsorption for ^{238}U available in this region (based on the measurement of the sum of the multiple $[>1]$ photoneutron cross sections) [13]. As one can see from this figure, no precise conclusions concerning the value of the fission probabilities can be drawn due to the large error bars of the total photoneutron cross sections.[1]

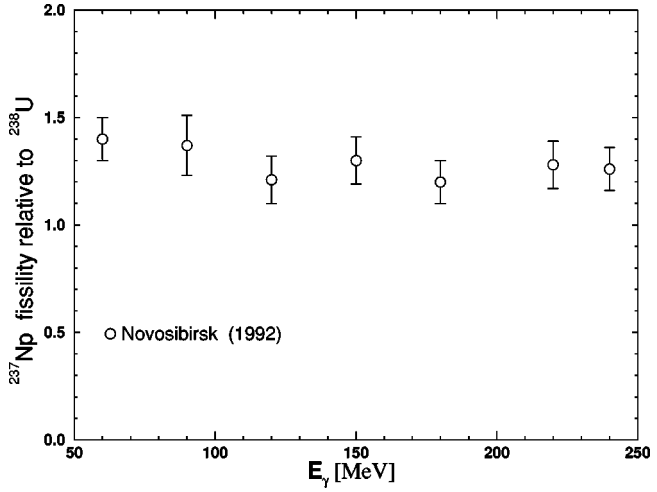

FIG. 2. Ratio of the ^{237}Np to the ^{238}U photofission cross sections [8].

In the Δ-resonance region (from about 150 MeV to 500 MeV), the total photofission cross sections for the actinides can be compared with the existing data on photoabsorption for nuclei from Li to Pb. These latter data have been obtained using a variety of experimental techniques, including the photohadronic technique, the transmission technique, and the measurement of neutron multiplicities [14–17]. The photohadronic technique consists in measuring the photoproduction rate of events at large angles (hadronic events), while rejecting the events whose products are emitted in the forward direction (electromagnetic events). The transmission technique consists in measuring the photon beam attenuation cross section and then subtracting the (calculated) atomic absorption cross section. The neutron-multiplicity technique consists in measuring the individual cross sections for the evaporation of multiple neutrons and then adding them to give the total cross section.

The existing data on photofission of ^{235}U and ^{238}U come from tagged-photon experiments at Bonn, Frascati, and Mainz [5–7]. From inspection of all these data, one can conclude that the total photofission cross sections per nucleon for ^{238}U and ^{235}U are close to each other and to the total photoabsorption cross section per nucleon for the light isotopes, and they all follow the so-called ''universal curve,'' which implies that the total photabsorption cross section is proportional to the number of nucleons inside the nucleus and hence to the nuclear volume. However, one can also notice that the uncertainty in the shape of the ''universal curve'' is of the order of at least 10% (not including the systematic uncertainties of all the measurements). This uncertainty has taken on increased importance in view of the results obtained at Novosibirsk on the photofission probabil-

[1]Especially when one adds the $(\gamma,1n)$, (γ,p), and possibly even (γ,α) cross sections not included in the $\sigma(\gamma,xn)$ results of Ref. [13].

ity of ^{237}Np relative to that of ^{238}U in the energy range between 50 and 240 MeV [8]. The relative fission probability of ^{237}Np seems to be at least 20% higher than that of ^{238}U, as shown in Fig. 2. This result thus contradicts the fundamental assumption that the fission probability for uranium at these energies is approximately equal to unity and that therefore the photofission cross sections for these isotopes are equivalent to the total photoabsorption cross sections.

Another interesting result in the photofission of actinide nuclei is the very different behavior of ^{232}Th from that of the heavier actinides at intermediate to high photon energies. Data below 100 MeV show that the fission probability (relative to ^{238}U) increases smoothly from 0.2 to 0.6 with photon energy [2]. Data at higher energies (from 250 to 1200 MeV) indicate that the fission probability (relative to ^{238}U), even at quite large photon energies, does not exceed approximately 0.8 and appears to saturate [18]. This high-energy behavior is not easy to understand; in spite of the scatter of the data, the average fissility is substantially lower than 1. This might show a strong dependence of the fission probability for actinides on atomic number and mass, specifically on the fissility parameter Z^2/A of the target nucleus.[2] Low-energy results also show that there is a transition to very low fission probability between thorium and radium [19]. Since the number of neutrons and protons escaping the nucleus during the intranuclear cascade increases with increasing photon energy, and because fission will occur with increased probability after several neutrons have been evaporated, an extrapolation from low energies is not justified. The fission probability of thorium is directly related to those for the uranium and transuranic isotopes. However, there are no data in the energy region between about 100 and 250 MeV; it is very important to bridge this gap, and to verify the absolute cross sections on both sides.

At photon energies appreciably higher than the peak of the Δ resonance (above 400 MeV), the most recent data on photofission and photoabsorption, from experiments at Frascati [6,18,17,20] and Mainz [4,5], show no evidence of excitation of the baryon resonances $D_{13}(1520)$ and $F_{15}(1680)$, which are clearly seen in the photon absorption cross sections for ^{1}H and ^{2}H as peaks at energies of $\sim$0.7 and $\sim$1.0 GeV. This unexpected behavior of these nucleon resonances in nuclei is still an open theoretical and experimental problem. It is important to have a thorough understanding of the relation between the total photoabsorption cross section and the photofission cross section for actinide nuclei at lower energies in order to understand these results.

In summary, the status of the previous data on photoabsorption and photofission for the actinides shows the necessity for a simultaneous measurement of both the absolute and the relative photofission cross sections for ^{235}U, ^{238}U, ^{237}Np, and ^{232}Th below and in the Δ-resonance energy region.

[2]The fissility parameter Z^2/A results from the competition between the Coulomb repulsion and the surface tension of the nucleus during the fission process.

C. Theory

The photofission of heavy nuclei, for photon energies higher than about 40 MeV, is described as a two-stage process. In the first stage (the fast stage[3]), the incident photon, with energy ω, initiates an intranuclear cascade in which some of the particles involved escape, leaving a new residual nucleus in an excited state, the so-called compound nucleus, which is characterized by the property that the excitation energy E_x is distributed over all possible degrees of freedom, such that thermodynamic equilibrium is established. The time scale of the formation of the compound nucleus is of the order of 10^{-19} s. In a second stage (the slow stage), the compound nucleus disposes of the excitation energy by gamma-ray emission, particle emission, or fission. The gamma-ray emission is important only when the excitation energy is below the threshold for particle emission or fission. Therefore, for highly excited heavy nuclei, the deexcitation process reduces to a competition between fission and particle emission. The emitted particles are mostly neutrons, although emission of protons, deuterons, trinucleons, and α particles is also possible, but far less probable because of the Coulomb barrier. The time scale of the deexcitation stage is of the order of 10^{-16} s.

The large difference between the time scales of the formation of the compound nucleus and its deexcitation justifies the description of the photofission process as a two-stage process. Based on this, one can write the cross section as [21]

$$\sigma_{\gamma,f}(\omega)=\sum_{A_C}\sum_{Z_C}\int_0^{\omega}\sigma_{CN}(A_C,Z_C;E_x)w_f(A_C,Z_C;E_x)\frac{dE_x}{\omega}, \tag{1}$$

where σ_{CN} is the cross section for the formation of the compound nucleus with A_C nucleons, Z_C protons, and excitation energy E_x, and w_f is the probability that the compound nucleus will fission in the transition to the ground state.

In Eq. (1), σ_{CN} summarizes the result of the fast stage of the fission process. The second term inside the integral in Eq. (1), w_f, describes the competition between particle emission and fission during the slow stage of the fission process. This quantity can be written as

$$w_f=\sum_k P_k(A_C,Z_C;E_x)w_k^f(A_C,Z_C;E_x), \tag{2}$$

where P_k is the probability that the compound nucleus will emit k particles in the transition to the ground state, and w_k^f is the probability that fission will occur in one of the k evaporative steps. These two quantities can be expressed in terms of the emission widths Γ_j for the set $\{j\}$ of all possible emitted particles $(j=n,p,d,t,^3\mathrm{He},\alpha)$ and the fission width Γ_f [21]. Therefore, based on this model, the determination of the fission probability of the compound nucleus reduces to the calculation of the partial decay widths Γ_j and Γ_f.

[3]The time scale of the direct reaction is of the order of 10^{-23} s.

For high-Z nuclei, neutron emission is much more probable than emission of charged particles, and thus w_f depends strongly on the ratio Γ_n/Γ_f. An expression for this ratio is given in Ref. [19]:

$$\frac{\Gamma_n}{\Gamma_f}=\frac{4A^{2/3}a_f(E-B_n)}{K_0 a_n[2a_f^{1/2}(E-E_f)^{1/2}-1]}\exp[2a_n^{1/2}(E-B_n)^{1/2} - 2a_f^{1/2}(E-E_f)^{1/2}], \quad (3)$$

where B_n is the neutron binding energy, E_f is the fission barrier, a is a nuclear level density parameter, and $K_0 = 14.39$ MeV. The parameters a_f and a_n describe the change in level density in the saddle point (large deformation) and in the ground state (smaller deformation) [19].

As one can see from Eq. (3), Γ_n/Γ_f has a strong dependence on a_n and a_f; thus, an accurate knowledge of these parameters for several isotopes is necessary for the description of the evaporative deexcitation and fission of a single target isotope. Unfortunately these are not very well known, either theoretically or experimentally, and one has to rely on semiempirical parametrizations of their dependence on A and Z.

An expression for a_n proposed by Iljinov *et al.* includes corrections due to excitation energy and shell effects [21]:

$$a_n=(0.134A-1.21\times10^{-4}A^2)\times\left[1+(1-e^{-0.061E_x})\frac{\Delta M}{E_x}\right]\ \mathrm{MeV}^{-1}, \quad (4)$$

where ΔM is the shell correction to the nuclear mass.

As for a_f, the parametrizations usually are expressed in terms of $r=a_f/a_n$. By fitting Eq. (3) to all the existing data on Γ_n/Γ_f for isotopes ranging from Sm up to U, and using a linear dependence of r on the fissility parameter Z^2/A, Martins *et al.* proposed the following expressions [22]:

$$r=1+0.05917(Z^2/A-34.34), \quad Z^2/A>34.90, \quad (5)$$

$$r=1+0.08334(Z^2/A-30.30), \quad 31.20<Z^2/A\leqslant 34.90, \quad (6)$$

$$r=1.281-0.01842(Z^2/A-20.00), \quad 24.90\leqslant Z^2/A\leqslant 31.20. \quad (7)$$

The complex dependence of Γ_n/Γ_f on A, Z, and E_x makes the results of these calculations very sensitive to the distributions $\Delta A(\omega)=A-A_C$, $\Delta Z(\omega)=Z-Z_C$, and $E_x(\omega)$ predicted by the intranuclear-cascade Monte Carlo models. While the distributions for ΔA and ΔZ are relatively sharp, the distribution for E_x becomes very broad as the photon energy increases, and its mean value tends to saturate for photon energies above 120 MeV [8,23]. This, plus the increase of the number of positive charges emitted by the nucleus, could explain the saturation of the photofission probability above the giant dipole resonance region.

II. EXPERIMENT

The goal of the present experiment was to measure the total photofission cross sections for the actinides ^{237}Np, ^{238}U, ^{235}U, ^{233}U, and ^{232}Th with 3% statistical precision and less than 5% systematic uncertainty. The experiment was performed at the Saskatchewan Accelerator Laboratory, using its photon-tagging facility. The targets of the aforementioned isotopes were irradiated with monochromatic real photons, and for each photofission event one of the two resulting fission fragments was detected. By counting the number of events that resulted in fission, and dividing that quantity by the number of incident photons, the total photofission cross sections were determined.

At SAL an electron beam incident on an aluminum radiator generates a bremsstrahlung photon beam. After the radiator, the electron beam is deflected away from the beam line by a dipole magnet, and the energy of each individual electron is measured by an array of scintillators located in the focal plane of the deflecting magnet (the photon tagger). The photons continue downstream and traverse a target foil. When a photofission event occurs, two fission fragments are emitted in opposite directions (the linear momentum transferred by a photon to a heavy nucleus is negligible in this energy range; therefore, the center-of-mass and laboratory frames are nearly the same). If one of the emitted fission fragments goes through the fission-fragment detector, the event is registered. The energy of the photon is determined from the difference in energy of the incident electron beam and the electron detected in the focal plane of the tagger. The electronic coincidence between the signal coming from the fission-fragment detector and one of the photon-tagger channels determines the experimental trigger.

As long as the target foils and the fission-fragment detectors are nearly transparent to the photon beam, one can place several target-detector pairs along the beam line, in order to measure simultaneously the photofission cross sections for different isotopes and/or to increase the statistics of the experiment by having several targets per isotope.

A. SAL electron accelerator and photon tagger

The electron accelerator at SAL consists of a linear accelerator (Linac) and a pulse stretcher ring (PSR). The PSR is designed to convert the pulsed electron beam of the Linac into an almost continuous beam. The energy range of the Linac goes from 50 MeV up to about 300 MeV, with a peak current of 200 mA. The PSR stretches the pulsed beam into a continuous beam, increasing its duty factor to nearly 100%. The range of energies of the PSR is the same as the Linac; however, its maximum current is limited to 70 μA [24].

In this experiment, the electron accelerator was operated at an energy of 287.7 MeV, so that the maximum photon energy coverage was achieved. During these measurements, the machine was operated at a relatively low current, to limit the number of accidental events coming from fission events induced by untagged low-energy photons [the photofission cross section for actinide nuclei peaks in the giant dipole resonance (GDR) region, where the bremsstrahlung yield is also very high].

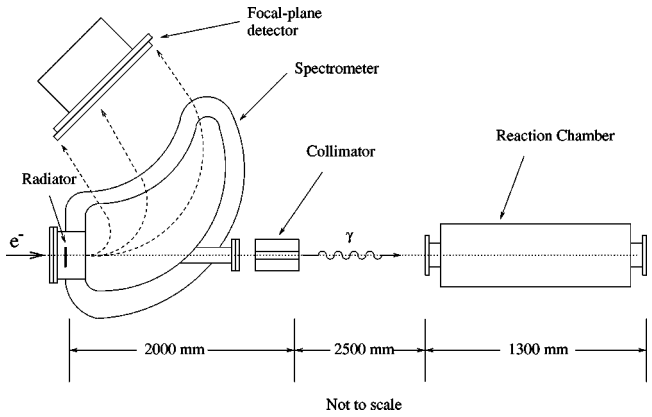

FIG. 3. Schematic diagram of the SAL photon tagger (not to scale).

The SAL photon-tagging facility consists of a radiator, an electron spectrometer, a focal-plane detector array, and a collimator. In Fig. 3 a schematic view of the system is presented. The focal-plane detector array consists of two rows of plastic scintillators. The first row has 31 scintillators, and the second one has 32. The two rows are shifted so that the scintillators in the first row overlap the scintillators in the second one by 50% [25].

Since the SAL photon tagger can tag photons only up to 223 MeV, a second spectrometer (''the end-point tagger''), located 1.8 m upstream from the first one, can be used to tag photons up to 264 MeV, using the same focal-plane detector array as the regular spectrometer (after being relocated).

In order to limit the spot size of the photon beam at the target, a lead collimator is located 2 m downstream from the radiator of the regular spectrometer. The diameter of the collimator was either 10 or 15 mm, and its length was 130 mm. The reaction chamber for the fission-fragment detectors and targets was located 2.5 m downstream from the collimator.

Only a fraction of the photons being radiated reaches the reaction chamber because of the collimator. This fraction is measured during special runs (tagging efficiency runs), in which a total-absorption lead-glass detector, located at the end of the photon beam line, is used to count the number of tagged photons in the collimated beam. The ratio of the number of tagged photons counted by the lead-glass detector and the number of electrons detected by the channels of the focal plane detector determines the fraction of photons that pass through the collimator. These tagging efficiency runs are performed regularly to account for possible changes in the electron beam profile and location. During these runs the fission detectors are removed from the photon beam line.

B. Fission-fragment detector system

For this experiment, the detectors of choice were parallel-plate avalanche detectors (PPADs) because they are known to be very efficient in detecting fission fragments. They are also ideal for photofission experiments because they have good time resolution (allowing the use of the photon-tagging technique), and they are practically insensitive to neutrons, photons, and electrons [26–33]. And although PPADs are sensitive to α particles, which are a common source of background when the targets are actinide nuclei, they provide good pulse-height discrimination between the α particles and the fission fragments.

PPADs were also ideal for this experiment because they can be quite transparent to an intense high-energy photon beam, allowing the location of a sizable array of target-detector pairs along the beam line. This is very important in order to increase the statistics of the measurements, a common problem for photofission experiments. It should also be pointed out that PPADs have a low production cost, as compared, for example, with solid-state detectors, allowing us to build many of them.

For this experiment, PPADs with anode wire grids were designed, built, and tested at The George Washington University Nuclear Detector Laboratory. The use of a wire grid for the detector anode instead of the usual thin foil of conducting material resulted in a higher detection efficiency because the fragments emitted from the target (located 17.5 mm away) were able to enter the active region of the PPAD without encountering any material (with the exception of those fragments that collided with the wires). Two collimators, one located right in front of the target and the other one located right in front of the detector, prevented fission fragments emitted at wide angles from being detected; in this way the distance traveled by the detected fragments inside the targets was minimized and the probability of reabsorption by the target material became negligible. At the same time the collimators prevented a large fraction of the α particles emitted by the radioactive targets from reaching the detectors, reducing significantly the main source of background in the experiment.

An array of target-detector pairs was placed inside a reaction chamber. The thin aluminum windows of the reaction chamber allowed the photon beam to pass through with very little attenuation. A target was placed in front of each PPAD. The targets were aluminum foils nominally 100 μm thick, with a film of fissionable material deposited on one side. A detailed description of the detectors and experimental setup is presented elsewhere [34,35].

C. Electronic readout and data acquisition

A schematic diagram of the experimental electronics is shown in Fig. 4. First, the signal from a PPAD is amplified and sent as input to a linear fanout module that splits it into two identical output signals. One of the output signals is delayed and used as input for the analog-to-digital converter (ADC).

The experimental trigger is defined by a logical OR among all the outputs of the constant-fraction discriminators (CFDs). In this way, as long as there is a signal in any of the PPADs, an *X-trigger* signal is produced. If the *X-trigger* signal is in coincidence with any of the tagger channels, the *X-ref* signal is sent back to the experimental electronics by the tagger interface, and is used as gate for the ADCs and the coincidence registers. It is also used as the start signal for the time-to-digital converters (TDCs).

Every time that an *X-ref* signal is produced, the tagger interface also sends a *LAM* (look at me) signal to the data-

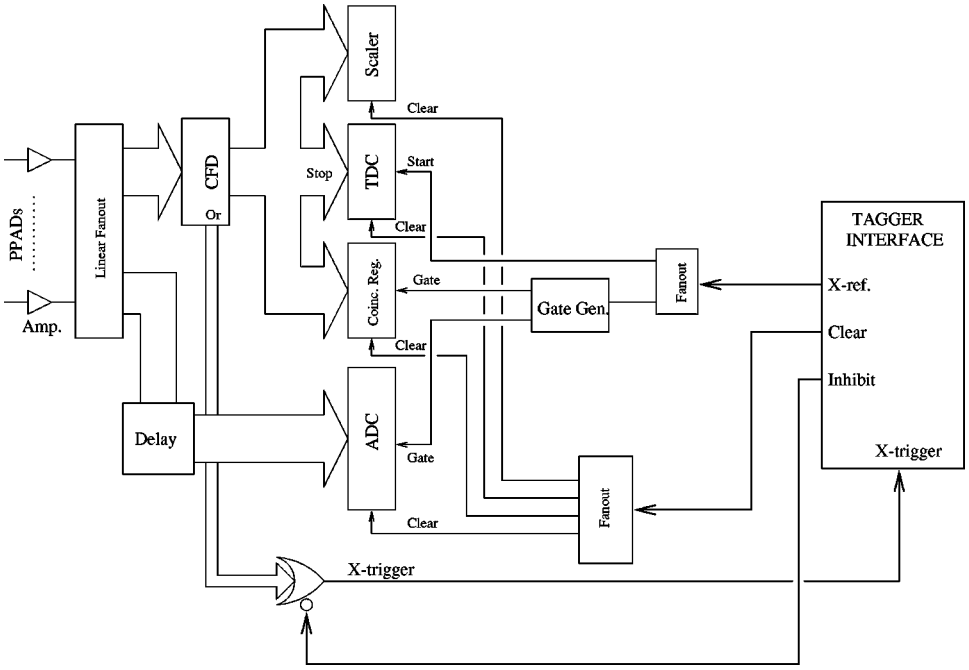

FIG. 4. Experimental electronics. For details, see text.

acquisition (DAQ) computer. In response to the *LAM* signal, the DAQ system reads out the contents of ADCs, TDCs, and coincidence registers.

D. Run summary

The experiment took place at SAL during the month of January of 1997. Table I shows the photon energy ranges covered during the experiment.

Data were recorded during intervals of approximately 2 h. Every 8 h, the reaction chamber was removed from the beam line and the total-absorption lead-glass detector was used to perform a tagging-efficiency run. These runs were divided into two parts. In the first part, the lead-glass counter would count all the photons that were not absorbed by the collimator, and whose signals were in coincidence with any tagger-channel signal. In the second part, the radiator would be removed from the beam line and the number of coincidences between the lead-glass detector and the tagger channels was measured. The events recorded during the second part can only be explained as the result of background in both detectors caused by the electron beam (the number of these events was always found to be negligible).

TABLE I. Photon energy ranges for the various tagger settings used in this experiment.

Setting	Tagger	E_γ^{min} [MeV]	E_γ^{max} [MeV]
1	Regular	68	146
2	Regular	128	189
3	Regular	161	206
4	Regular	182	223
5	End point	218	247
6	End point	234	257
7	End point	248	264

The photon-tagging rate was kept at about 4×10^6 photons per second, and the average tagging efficiency was 45% for the regular tagger (collimator diameter $=10$ mm) and 40% for the end-point tagger (collimator diameter $=15$ mm). The reason the latter is lower is that the end-point tagger is further from the collimator. The pressure of the reaction chamber was 15 Torr, and the voltage applied to the detectors was 750 V. During the experiment three targets of ^{238}U, ^{235}U, ^{237}Np, and ^{232}Th, and four of ^{233}U were installed inside the reaction chamber. A ^{252}Cf source and a dedicated PPAD were also included, positioned out of the photon beam line, so that they could act as a monitor of the performance of the other PPADs. Two aluminum targets of different thicknesses were included in order to study the effect of this material present in the targets (the fissionable material is deposited on 100-μm-thick aluminum foils). For details, see Refs. [34,35].

III. DATA REDUCTION

The experimentally measured total photofission cross sections are proportional to the ratio of fission events and tagged photons. The number of fission events is determined from the coincidence between signals from PPADs and tagger detectors (having subtracted the background events resulting from accidental coincidences and α particles). Corrections to this number have to be made to account for the fraction of solid angle not covered by the detectors and for the detection efficiency of the PPADs. The number of tagged photons is evaluated by counting the number of electrons detected at the focal plane of the tagger, and then corrected for those photons absorbed by the collimator (the tagging efficiency). Therefore, the photofission cross sections were determined using the following equation:

$$\sigma^l(E_k)=\left(\frac{4\pi}{N_0}\right)\frac{A^l}{t^l\epsilon^l_{\rm DET}\Omega^l_{\rm DET}}\,\frac{Y^l_k}{N_k\epsilon^{\rm TAG}_k}\times10^{30}\quad[\rm mb]\quad(8)$$

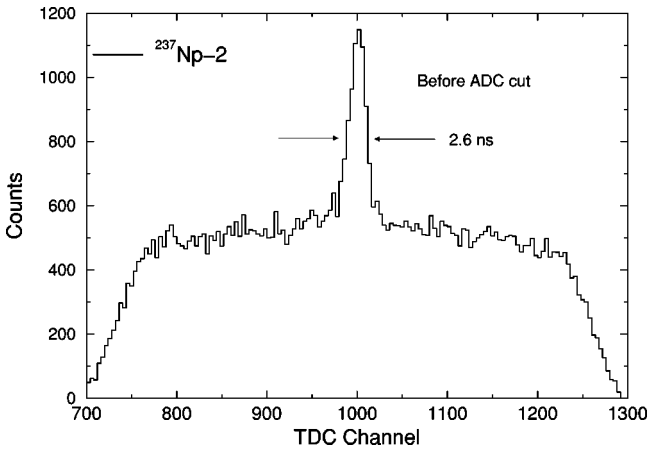

FIG. 5. Tagger TDC spectrum for the target ^{237}Np-2 before ADC cut.

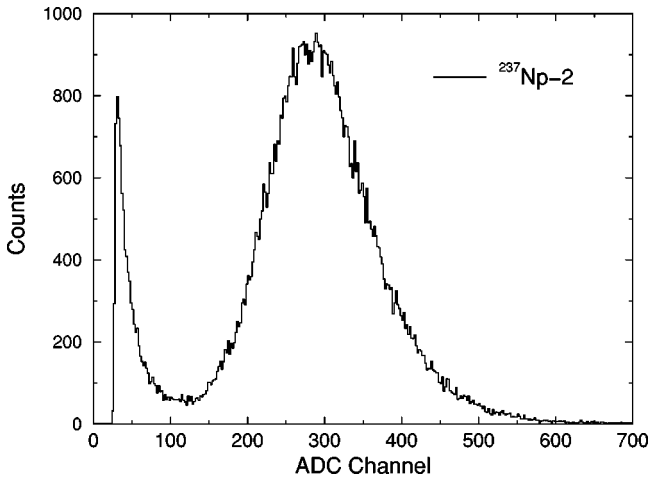

FIG. 6. ADC pulse-height spectrum for the target ^{237}Np-2.

where l is the index that runs over targets, k is the index that runs over tagger channels, E is the photon energy associated with a tagger channel [MeV], N_0 is Avogadro's number [atoms/mol], A is the target atomic weight [g/mol], t is the target thickness [mg/cm^2], ϵ_{DET} is the detector efficiency, Ω_{DET} is the detection solid angle [sr], ϵ^{TAG} is the tagging efficiency, Y is the yield of fission events induced by tagged photons, and N is the number of tagged photons.

The photon tagger covers only a fraction of the bremsstrahlung spectrum. By changing the field of the magnet and the position of the focal-plane detector array, different energy regions can be spanned. A first magnet (''regular tagger'') can tag photons up to $\sim$223 MeV. In order to tag higher-energy photons, a second magnet is used (''end-point tagger'') with the same focal-plane detector array. In Table I the photon energy ranges used during the experiment are listed. For each tagger setting there are 62 energy channels. The calibration of the energy covered by each channel was performed previously by the SAL staff.

To determine the number of fission events induced by tagged photons, the basic information comes from the TDC spectrum of each tagger channel. The TDC is started by the *X-trigger* signal coming from a PPAD and it is stopped by a signal in the tagger channel. The event is accepted and read out by the DAQ system if the two signals are within a given resolving time (60 ns in this case). The resolving time should be long enough so that a significant portion of the random coincidence spectrum is recorded, studied, and subtracted.

In many cases the signal in the PPAD is produced either by a fission event induced by an untagged photon or by an α particle. For such events (accidental coincidences), the fact that the PPAD signal might be in coincidence with the signal from a tagger channel is an accident. However, there is no time correlation between those two signals, and these kinds of events therefore produce a flat background in the TDC spectrum.

When the PPAD signal is the result of a fission event induced by a tagged photon, there is a time correlation between this signal and the signal produced in one of the tagger channels by the corresponding electron. These kinds of events (true coincidences) will appear in the TDC spectrum as a narrow peak with a width of about 2.5 ns, which is the combined resolution time of the PPADs and tagger channels.

Figure 5 shows the TDC spectrum for one of the ^{237}Np targets. In this example the contributions of all the tagger channels have been combined to enhance the statistics.

The coincidence peak rests on top of a pedestal of random coincidences. To subtract the background under the peak, one interpolates between the background levels on both sides of the peak. For this analysis, the level of background was evaluated by taking the average of the number of counts in regions very close to the coincidence peak, in order to minimize the effect of any structure in the distribution of background. There is an uncertainty associated with any background subtraction procedure, but as we will see later, in this case its magnitude is within the accuracy of our measurements, and therefore there is no need to implement a more sophisticated procedure.

In principle, the TDC spectra are the only data needed to determine the number of tagged fission events. However, the energy information stored in the PPAD ADC spectra can be used to reduce the level of background, and thus to facilitate its subtraction. In Fig. 6 a typical ADC spectrum is presented. The decaying distribution in the low-energy part is the contribution of the α particles, and the large central peak results from the fission fragments (tagged and untagged). The two distributions overlap due to the wide collimation. In spite of the overlap, one can still reject the events whose ADC channel number is low enough so that it cannot be the result of a fission fragment, for example, in the case of Fig. 6, events whose ADC channel number is below $\sim$75. In this way most of the α particles are eliminated from the data.

The number of tagged photons is equivalent to the number of electrons detected by the channels of the tagger focal-plane detector array. The event rate per channel is registered by the scalers of the tagger electronics (they are read out by the DAQ system every 10 s). The sum of all the scaler readings over a period of time represents the number of tagged photons per channel over that period. Of the photons that are tagged, only about half strike the target samples. The rest are absorbed in a thick lead collimator with an aperture diameter of 10 mm, located 2 m downstream from the aluminum ra-

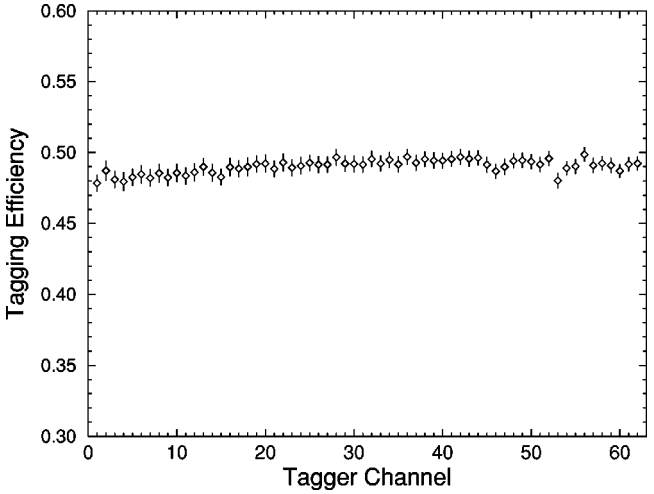

FIG. 7. Result of a typical tagging efficiency run.

diator in the case of the regular tagger, and a 15-mm lead collimator located 3.9 m downstream from the aluminum radiator in the case of the end-point tagger (both collimators were 130 mm thick). All other sources of inefficiency, such as electronic noise in a focal-plane detector, were negligible by comparison. The tagging efficiency was determined during special runs in which the tagger was put in coincidence with the lead-glass photon detector positioned in the photon beam line 4 m downstream from the fission chamber. Immediately after each of these normalization runs, the aluminum radiator was removed from the beam line and background data were recorded. In this way the level of background coming from the tagger spectrometer was measured and found to be minimal. The efficiency of each of the 62 channels of the photon tagger was evaluated using

$$\epsilon_k^{\mathrm{TAG}} = \frac{Y_k^{\mathrm{IN}}}{N_k^{\mathrm{IN}}}, \tag{9}$$

where N_k represents the number of electrons detected in the kth channel of the tagger, Y_k represents the number of those events detected in coincidence with the lead-glass detector, and the superscript ''IN'' represents the status of the aluminum radiator with respect to the beam line. The result of a typical normalization run is shown in Fig. 7.

In order to determine the geometrical acceptance of the target-detector pairs, a Monte Carlo calculation was performed. This calculation included electron-beam spot size, the angular distribution for the bremsstrahlung photons, the effect of the photon-beam collimator, the isotropic distribution of fission fragments emitted by the target, and the effect of any collimators between the target and the PPAD. In this way the size of the photon-beam spot at the position of each target was accounted for. The effective solid angle covered by the PPAD was then determined to be $\Omega_{\mathrm{DET}} = 0.39 \times 4\pi$ sr.

A PPAD is a very efficient fission-fragment detector. Most of the inefficiency comes from the wire grid that forms the anode plane. The collimators limit the angles at which the particles enter the active region; therefore, the inefficiency is approximately equal to the fraction of the area blocked by the wires, which is 2%, resulting in a detection efficiency of 0.98. Since the accepted fission fragments were emitted in the direction normal to the plane of the target (due to the collimation), the distance that they traveled inside the film of fissionable material was minimized. A detailed study of the existing data on the range of typical fission fragments traveling through uranium showed that the fraction of fragments reabsorbed by the film is negligible.

TABLE II. Thicknesses of the targets used in this experiment, as measured by their α activities.

Target	Technique	Thickness [mg/cm^2]
^{232}Th-1	Counting rate	1.25±0.02
^{232}Th-2	Counting rate	1.23±0.02
^{232}Th-3	Counting rate	1.23±0.02
^{233}U-1	Energy loss	0.62±0.02
^{233}U-2	Energy loss	0.65±0.02
^{233}U-3	Energy loss	0.57±0.02
^{233}U-4	Energy loss	0.58±0.02
^{235}U-1	Energy loss	0.89±0.03
^{235}U-2	Energy loss	0.93±0.03
^{235}U-3	Energy loss	1.07±0.04
^{238}U-1	Counting rate	1.48±0.03
^{238}U-2	Counting rate	1.61±0.03
^{238}U-3	Counting rate	1.23±0.02
^{237}Np-1	Counting rate	0.94±0.02
^{237}Np-2	Counting rate	0.99±0.02
^{237}Np-3	Counting rate	0.93±0.02

The targets consist of thin layers of actinide isotopes deposited on aluminum foils 100 μm thick. The dimensions of the foils are 12 cm long and 6 cm wide. Only a central circle of 4 cm in diameter was exposed to the photon beam. In order to accurately determine the thickness and composition of the film, a measurement of the rate and energy spectrum of the α activity for each target was performed at SAL. Each individual target was placed inside a vacuum chamber and the α particles were detected with a silicon surface barrier detector. Scaler and ADC information was recorded. In order to get an energy calibration, data were also recorded for ^{210}Po, ^{241}Am, and ^{252}Cf sources. The energy resolution of this setup was approximately 30 keV, allowing us to identify the different isotopes present in the samples with no ambiguity. By measuring the rate of α particles of a given isotope emitted from a particular region of the foil in a particular solid angle, we were able to determine the amount of that isotope in the sample. With this technique we determined the thicknesses of our ^{232}Th, ^{238}U, and ^{237}Np films. For the cases of ^{233}U and ^{235}U the presence of ^{234}U and ^{238}U contamination did not allow us to use the counting-rate technique. For these targets we used the information provided by the ^{232}Th, ^{237}Np, and ^{238}U films (whose thicknesses we had determined already) to establish a relation between the ADC-spectrum width and the film thicknesses for different isotopes, determining in this way the thickness of the ^{233}U and ^{235}U samples. Table II summarizes the results of our mea-

surements. A detailed description of the target-thickness measurements can be found elsewhere [35,36].

As mentioned in the previous section, the films of fissionable material were deposited on aluminum foils, 100 μm thick. In order to measure the contribution of this material to the fission-fragment yield, aluminum foils were included in the reaction chamber. The reaction cross sections for these samples were measured using the same procedure as for the targets. The contribution of the aluminum substrate to the fission yields was determined to be of the order of 10^{-3}%; therefore its effect on the measured photofission cross sections was negligible.

The efficiency and the solid-angle acceptance of the detectors have been calculated numerically. As was mentioned above, these calculations include all the elements that could have an effect on the results. The uncertainties associated with these calculations have been estimated to be less than 1% for both quantities.

The tagging efficiency has been measured to a statistical uncertainty of 1%. Any systematic uncertainty associated with the procedure comes from the fact that the accelerator electron current is decreased during the tagging efficiency runs. (This is done in order to keep from overloading the lead-glass detector.) The physicists at SAL have performed this kind of measurement for several years and for many different experiments, and their observations indicate that the effect of the beam current reduction is small. We estimate the uncertainty in the knowledge of the tagging efficiency for this experiment to be 2%.

The uncertainty associated with the background-subtraction procedure is caused by the structure of the TDC distribution of random coincidences (see Fig. 5). If this distribution were perfectly flat, there would be no systematic uncertainty in the interpolation that was done to determine the level of background under the coincidence peak. However, the presence of time-dependent structure in the distribution makes the procedure somewhat less accurate.

The level of background under the coincidence peak in the TDC spectrum for each PPAD was determined by measuring the average number of events per channel in the two regions adjacent to the coincidence peak. The boundaries defining the coincidence peak and the two adjacent background regions were selected individually for each PPAD and each data set (20 PPADs and 26 data sets). By choosing different sets of boundaries, and studying the changes in the background levels, the effect of this procedure on the final cross sections was evaluated. The background subtraction studies showed that the change in the average cross sections due to different choices of background levels (within reasonable limits) was at most 3%.

IV. RESULTS

A. Total photofission cross sections

Following the methods presented in the previous section, the total photofission cross sections for each target and each tagger setting were measured. The cross sections for the targets of the same isotope were then combined. In Figs. 8 and 9, our measured total photofission cross sections for the actinide isotopes are presented. From these figures one can see that all the cross sections show a similar energy dependence. They are approximately constant up to 100 MeV photon energy (in the quasideuteron region), and then the rise of the Δ resonance is clearly observed. There is no clear evidence of any other energy-dependent structure, especially above the pion-production thresholds. The most important feature of the results is the significantly higher cross section for ^{237}Np when compared with ^{238}U, and even with ^{235}U. The cross section for ^{232}Th is much lower than the ones for the other actinide isotopes; this was expected from previous results at lower and higher energies. Smaller differences among the uranium isotopes are also noticeable. In the next section these results will be analyzed in more detail, and compared with existing data and calculations.

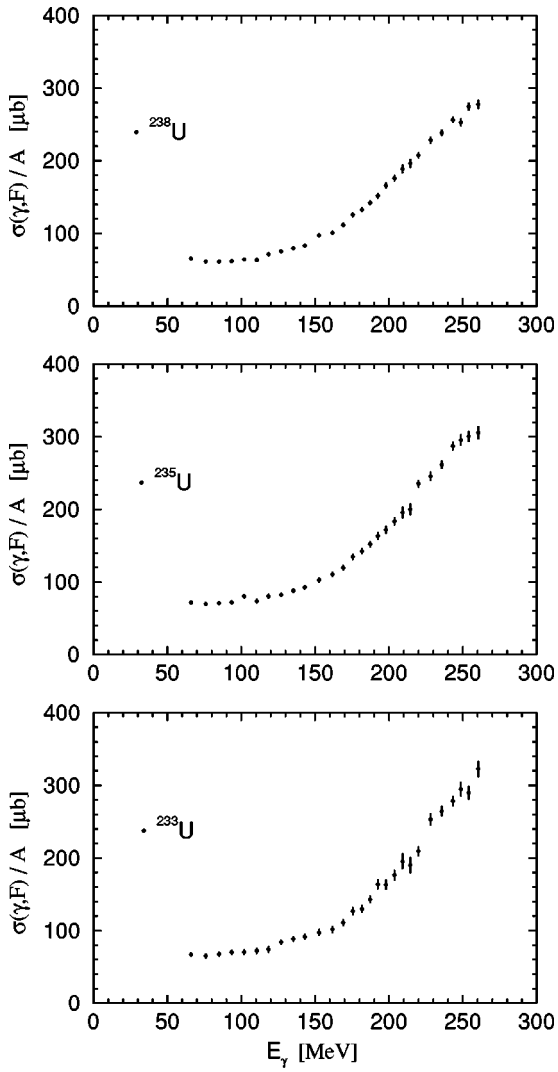

FIG. 8. Photofission cross sections per nucleon for the uranium isotopes measured in this experiment.

To test the self-consistency of the results, the cross sections for the different targets and different tagger settings were compared. The data for the different settings always fell within the statistical uncertainties of the measurements, as did the data for the different targets of the same isotope. The data from the two taggers used in the experiment, the ''regu-

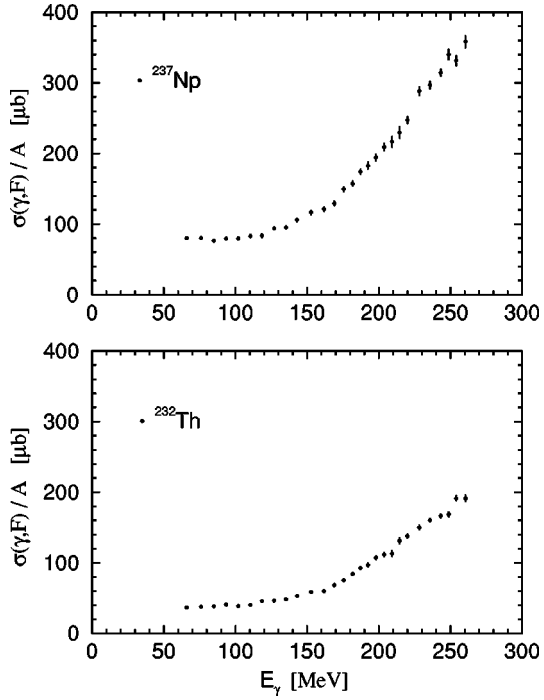

FIG. 9. Photofission cross sections per nucleon for ^{232}Th and ^{237}Np measured in this experiment.

lar tagger'' and the ''end-point tagger,'' also matched in the overlapping region. The data from the end-point tagger are slightly more scattered, probably the result of the presence of somewhat higher backgrounds in the focal-plane detector array for this spectrometer. To double-check the normalization among different targets of the same isotope, the average cross sections over the measured photon energy range were calculated and compared. From these results we notice that the ^{233}U and ^{235}U cross sections have a larger standard deviation than the others. This difference probably results from the uncertainty in the target-thickness determination, since for these two isotopes the target thickness was measured using the energy-loss technique, in contrast with the other isotopes, for which the thickness was determined using the α activity technique. In the case of ^{233}U, it is also important to note that the level of background was much higher than for the other isotopes due to its very high α activity. The systematic uncertainties for each cross section are listed in Table III.

TABLE III. Systematic uncertainties for the photofission cross-section measurements.

Isotope	Y_k	ϵ^{TAG}	Ω_{DET}	ϵ_{DET}	t^l	Total
^{232}Th	1.5%	2%	<1%	<1%	2.0%	3.5%
^{233}U	2.5%	2%	<1%	<1%	3.5%	4.9%
^{235}U	2.5%	2%	<1%	<1%	3.5%	4.9%
^{238}U	2.0%	2%	<1%	<1%	2.0%	3.7%
^{237}Np	1.8%	2%	<1%	<1%	2.0%	3.6%

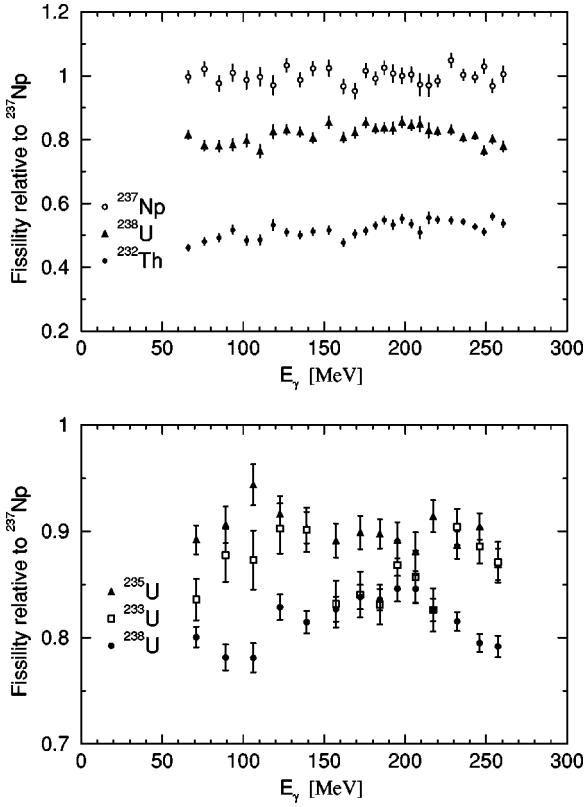

FIG. 10. Fissilities relative to ^{237}Np measured by this experiment. The ratios of the ^{237}Np data relative to the fitted curve are shown as well, so that one can assess their scatter.

B. Relative fissilities

Traditionally the fissilities of the actinide isotopes have been presented relative to ^{238}U by dividing the total photofission cross section of the isotope by the total photofission cross section of ^{238}U. However, since the cross section for ^{237}Np is now seen to be higher, it makes more sense to present the fissilities relative to this isotope. To do this, a fifth-order polynomial was fitted to the ^{237}Np cross section, and then the other cross sections were divided by this function. Figure 10 shows the fissilities of the actinide isotopes relative to ^{237}Np.

Two important features of the results are the very weak dependence of the fission probability on photon energy and its strong dependence on the fissility parameter Z^2/A (of the target isotope). The differences in fissility between ^{237}Np, ^{238}U, and ^{232}Th are very well established (see Fig. 10). Less important differences are observed among the uranium isotopes: the fissility of ^{235}U is highest and that of ^{238}U is the lowest.

C. Cross-section fits

Polynomial fits of fifth order to all the measured total photofission cross sections were performed in order to assess differences in shape and absolute value of the cross sections for the different isotopes. The χ^2/N_{df} did not exceed 1.3 for

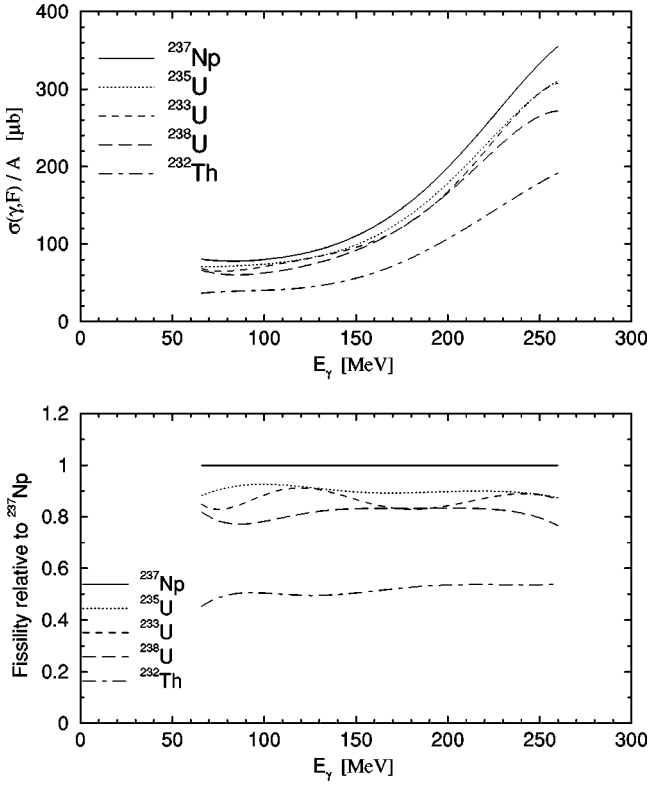

FIG. 11. Fits to the photofission cross sections per nucleon and relative fissilities. Caution should be exercised in assessing these curves; one must remember to attach an appropriate error band to each. The scatter in the actual data can be seen in Figs. 8, 9, and 10.

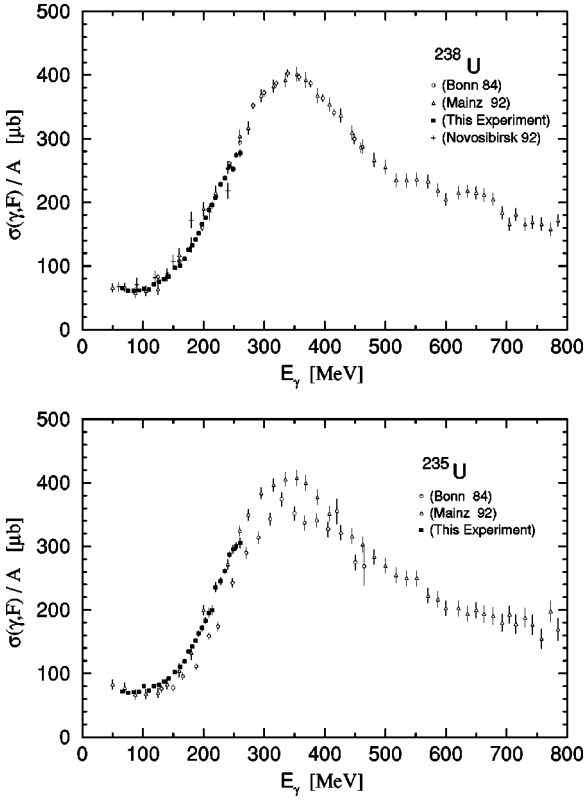

FIG. 12. Photofission cross sections per nucleon for ^{238}U and ^{235}U compared with those from previous measurements.

any of the isotopes, with the exception of ^{232}Th. These results reflect the smooth behavior of the cross sections as functions of energy. In the case of ^{232}Th, the χ^2/N_{df} was 2.25, which may just be related to the fact that for this isotope the statistical accuracy of the data was far better than the systematic uncertainty of the measurement. Fissilities relative to ^{237}Np were calculated by dividing the polynomial for each isotope by the polynomial for ^{237}Np. The total photofission cross sections and relative fissilities calculated in this way are shown in Fig. 11. In assessing these fitted curves, one must remember to attach an appropriate error band to each, especially the fissility curves. The scatter in the actual data can be seen in Fig. 10.

V. ANALYSIS AND INTERPRETATION

A. Total photofission cross sections

The total photofission cross sections for ^{238}U and ^{235}U have been measured by experiments at Bonn and Mainz in the energy range of our experiment [7,5]. The cross section for ^{238}U was also measured at Novosibirsk [8]. In Fig. 12 the results of these measurements are compared with ours. In the case of ^{238}U the agreement among the different sets is excellent, while for ^{235}U the data from the earlier Bonn experiment are systematically lower than those from the recent Mainz experiment and from the present experiment, which are in excellent agreement with each other.[4] Our results also agree with those from Saclay [2] at lower energies.

The total photofission cross section for ^{237}Np measured in this experiment is compared in Fig. 13 with the only other measurement, performed at Novosibirsk [8]. Even though the two results do not agree in detail (the Novosibirsk data are systematically higher), both experiments have found the ^{237}Np cross section to be substantially larger than that for ^{238}U.

Also, as can be seen in Fig. 13, for the case of ^{232}Th, the results of our experiment match well with the existing data at lower and higher energies [2,18]. Our measurement thus fills the previously existing gap on the low-energy side of the Δ resonance.

B. Photoabsorption cross sections

The total photofission cross section for ^{238}U is $\sim$20% lower than that for ^{237}Np. This means that if either of these cross sections is a good approximation to the absolute photoabsorption cross section, it must be the one for ^{237}Np.

In Fig. 14 one can see that the total photofission cross section for ^{238}U intersects the photoabsorption cross section for Be, while the total photofission cross section for ^{237}Np is higher. One also notices that the slope of the Be cross section

[4]Note that the systematic uncertainties of these measurements are not included in the error bars. In the case of the Mainz and Bonn data they are of the order of 8%.

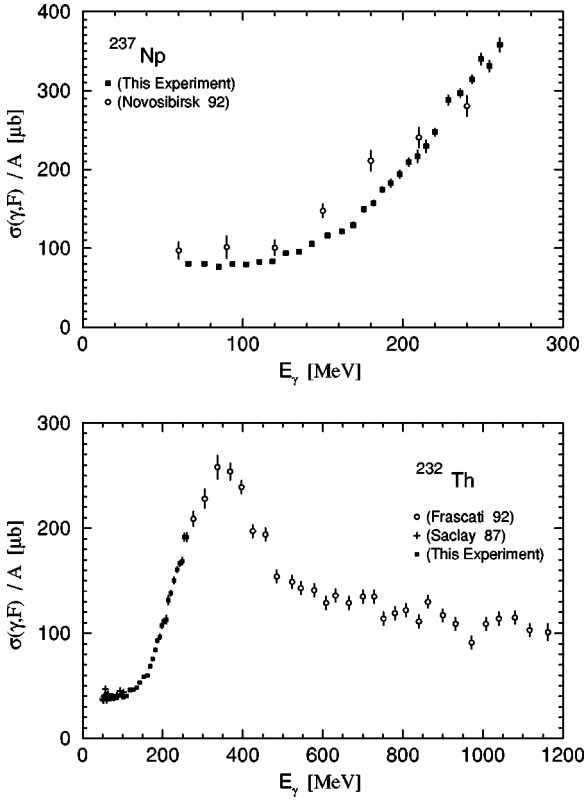

FIG. 13. Photofission cross sections per nucleon for ^{237}Np and ^{232}Th, compared with those from previous measurements.

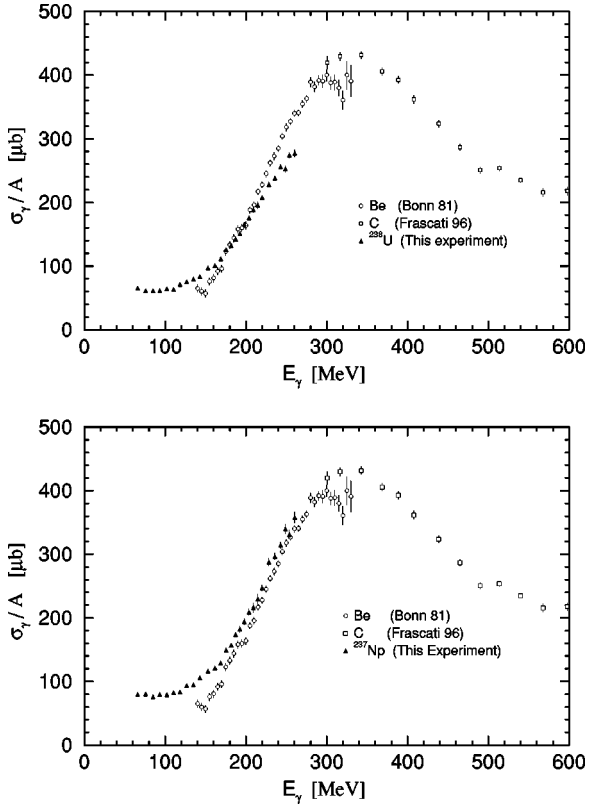

FIG. 14. Photofission cross sections per nucleon for ^{238}U and ^{237}Np, compared with photoabsorption cross sections for Be and C.

is steeper than those of the actinides. If one discards the cross section for ^{238}U and assumes the one for ^{237}Np as an approximation to the total photoabsorption cross section for heavy nuclei, the results are in agreement with microscopic models that predict a broadening of the Δ resonance for heavy nuclei [37]. This suggests that the fission probability for ^{237}Np is close to unity. However, as we will discuss in the next section, not until an actual photoabsorption measurement for actinide isotopes with larger Z^2/A is performed can one be sure of the validity of such an assumption.

C. Fission probability

From the relative fissility results presented in the previous section, two important features should be noticed: that the fission probability is almost constant in this energy range and that the relative fissilities are an increasing function of the fissility parameter Z^2/A of the target isotope. This latter feature is shown in Fig. 15, which is a plot of the relative fissility on a linear scale.

In order to understand the nature of these results, a calculation of the fission probability was undertaken. The calculation is divided into two parts, the intranuclear cascade and the evaporation cascade. At the intranuclear-cascade level, the goal is to describe as accurately as possible the distributions of E_x, ΔA, and ΔZ. These distributions, as functions of photon energy, were taken from the intranuclear-cascade calculations presented in Ref. [8]. At the evaporation-cascade level, the models for fission and neutron evaporation presented in the first section were implemented. The parameter for the density of energy levels at the saddle point relative to the one for the neutron at the ground state of nucleus deformation was assumed to be of the form

$$\frac{a_f}{a_n} = 1 + \alpha\left(\frac{Z^2}{A} - \beta\right), \tag{10}$$

following the same parametrization suggested in Ref. [22]. The parameters α and β were adjusted to fit our data, and their best values were $\alpha = 0.14$ and $\beta = 32.94$.

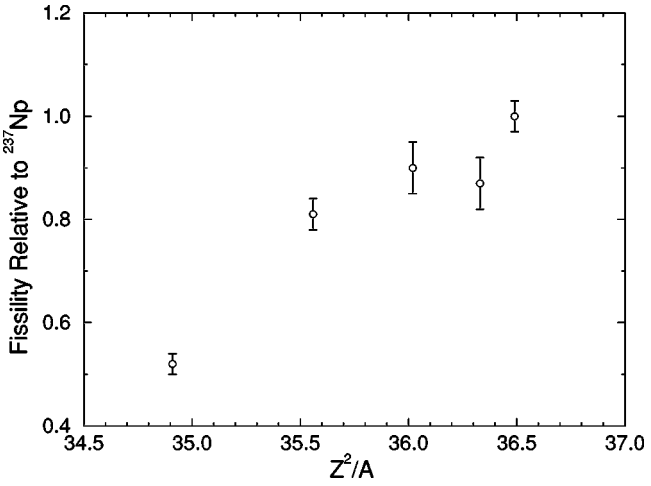

FIG. 15. Fissility as a function of the fissility parameter of the target for ^{232}Th, ^{238}U, ^{235}U, ^{233}U, and ^{237}Np (in order of increasing Z^2/A).

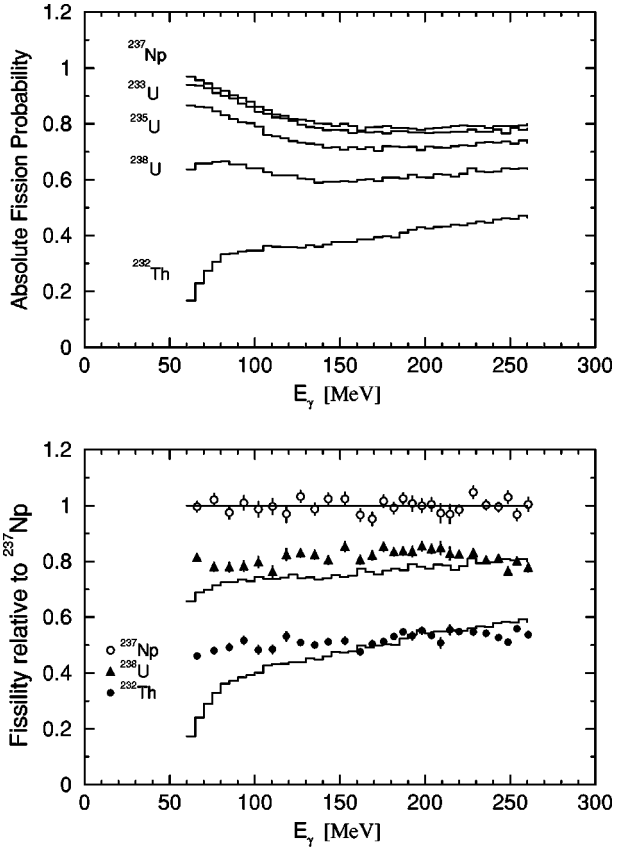

FIG. 16. Top: fission probability for ^{237}Np, ^{233}U, ^{235}U, ^{238}U, and ^{232}Th calculated from a liquid-drop model. Bottom: comparison of the relative fissilities for ^{237}Np, ^{238}U, and ^{232}Th.

The evaporation of n, p, d, t, ^{3}He, and α particles was included. The values for their Coulomb barriers and level density parameters were taken from Ref. [38]. Figure 16 shows the results of the calculation, and compares these results with the experimental data.

From the calculation one can notice that the fission probability for the more fissile isotopes decreases in the energy range between 50 MeV and 150 MeV, and then it tends to flatten out. This effect is the result of charged-particle emission during the intranuclear cascade, especially proton emission, which has the greatest negative impact on the fissility parameter Z^2/A of the compound nucleus. The distributions of emitted particles published in Ref. [8] show that the average number of emitted protons and neutrons saturates above 140 MeV. This is because, as pions start being produced inside the nucleus, the kinetic energies of the secondary particles in the absorption reaction (the pion and a nucleon) are relatively small, and the chance of any of them escaping decreases. The results of the model are very sensitive to the average number of protons emitted (the more protons emitted, the lower the fission probability). One must also realize that, as the photon energy increases, the excitation energy becomes a broader distribution, and a larger number of events leave a small excitation energy in the compound nucleus (most of the energy of the incoming photon is carried away by the emitted particles, something that does not happen at lower energies).

During the evaporation cascade, the probability of evaporation increases with nuclear temperature, as well as the amount of energy carried away by the evaporated particles. Also, the relative probability of emission of charged particles becomes significant, having a noticeable impact on the fission probability of the remaining (residual) nucleus.

There are many parameters and many approximations in these kinds of calculations, but the gross features of their results tell us something about their nature. It seems that the saturation of the fission probability can be explained as a consequence of the many competing processes. The absolute value of the fission probabilities predicted by this model may depend on the various assumptions and parameters; however, when one takes the ratio between two fission probabilities (relative fissility), most of these effects become much less important. Figure 16 also shows that the calculated relative fissilities (except that for ^{233}U) scale properly when compared with the data. In Fig. 15 the average fissility for the actinide isotopes is plotted as a function of the fissility parameter Z^2/A. The dependence of this quantity on the fissility parameter can be explained as the result of the direct dependence of a_f/a_n on that parameter [Eq. (10)]. One can conclude that the photofission probability, even in this relatively high-energy range, has an important dependence on the density of energy levels of the nucleus.

One unexpected result of this experiment is the somewhat higher fissility of ^{235}U relative to ^{233}U, which is contrary to the results at giant-resonance energies of Refs. [10] and [12]. According to the liquid-drop model, the fission probability for ^{233}U should be higher than that for ^{235}U. However, shell-model corrections to fission and to particle evaporation might be important at this level of accuracy, and our calculations do not include any. Also, the fissility parameters for these two isotopes are very similar, and the systematic uncertainties in our cross-section measurements for these two isotopes are higher than for the rest, due to the target-thickness determination and the background subtraction.

VI. CONCLUSIONS

The total photofission cross sections for ^{237}Np, ^{238}U, ^{235}U, ^{233}U, and ^{232}Th have been measured in the quasideuteron and the lower part of the Δ-resonance regions. From the analysis of these data and their comparison with previous results, we draw the following conclusions.

(i) We have observed that in this energy range the fission probability for ^{237}Np is significantly higher than the fission probability for ^{238}U (by $\sim$20%), in qualitative agreement with the result from Novosibirsk [8].

(ii) Our results for the total photofission cross sections for uranium isotopes are generally in good agreement with previous results, especially with those from Mainz [5].

(iii) The total photofission cross section for ^{232}Th matches very well with the results at lower and higher energy from Saclay and Frascati [2,18], respectively.

(iv) The relative fissilities for the uranium and transuranic isotopes are constant in this energy range, which suggests that the fission probability, as a function of photon energy,

saturates at a value that increases with the fissility parameter of the target isotope.

(v) For the less fissile isotope ^{232}Th, the fission probability increases slightly with increasing energy, and seems to be tending towards a saturation value at somewhat higher energies. This indicates that, for all the isotopes, a saturation value is eventually reached.

(vi) The comparison between the total photofission cross section for ^{237}Np (the isotope with highest fissility measured by us) and the photoabsorption cross section for Be is consistent with a broadening of the Δ resonance for heavy nuclei.

(vii) The total photofission cross section for ^{238}U intersects the photoabsorption cross section for Be in the low-energy tail of the Δ resonance. This result and that for ^{237}Np, evidence that the photofission cross section for ^{238}U is not a good approximation (at the 10% level) to the photoabsorption cross section for heavy nuclei.

(viii) If one assumes that the total photofission cross section for ^{237}Np is a good approximation to the photoabsorption cross section for heavy nuclei (bearing in mind that even it may be lower), one concludes that the photoabsorption process has a noticeable dependence on atomic mass. This result calls into question the conceptual reach of the so-called ''universal curve.''

(ix) The saturation of the fission probability below unity, even for very fissile nuclei like the uranium isotopes, prevents one from concluding that the photofission cross section for ^{237}Np is equal to the photoabsorption cross section. The dependence of the relative fissility on the fission parameter suggests that the maximum fissility could be higher still. A measurement of the photofission cross section for ^{239}Pu would be valuable.

ACKNOWLEDGMENTS

The authors are grateful to the Saskatchewan Accelerator Laboratory staff, in particular to its director Professor Dennis Skopik for his support to this project from its inception, to the engineering staff for the design and construction of all the necessary structures and instruments to install our detectors, and to the technical and accelerator operations staff for their unconditional commitment to the experiment during its running period. The authors also acknowledge the contributions of Dr. William Dodge, Professor Mark Reeves, Dr. Scott Matthews, Henrik Ayvazian, and William Rutkowski, who provided many ideas for this experiment. The work at The George Washington University was supported by U.S. DOE Grant No. DE-FG02-95ER40901.

[1] H. Ries *et al.*, Phys. Lett. **139B**, 254 (1984).
[2] A. Leprêtre *et al.*, Nucl. Phys. **A472**, 533 (1987).
[3] J. Ahrens, Nucl. Phys. **A446**, 229c (1985).
[4] Th. Frommhold *et al.*, Phys. Lett. **127B**, 331 (1983).
[5] Th. Frommhold *et al.*, Z. Phys. A **350**, 249 (1994).
[6] N. Bianchi *et al.*, Phys. Lett. B **299**, 219 (1993).
[7] J. Ahrens *et al.*, Phys. Lett. **146B**, 303 (1984).
[8] A. S. Iljinov *et al.*, Nucl. Phys. **A539**, 263 (1992); also see G. Ya. Kezerashvili *et al.*, JETP Lett. **40**, 1271 (1984).
[9] A. Veyssière *et al.*, Nucl. Phys. **A199**, 45 (1973).
[10] J. T. Caldwell *et al.*, Phys. Rev. C **21**, 1215 (1980).
[11] H. Ries *et al.*, Phys. Rev. C **29**, 2346 (1984).
[12] B. L. Berman *et al.*, Phys. Rev. C **34**, 2201 (1986).
[13] A. Leprêtre *et al.*, Nucl. Phys. **A367**, 237 (1981).
[14] J. Arends *et al.*, Phys. Lett. **98B**, 423 (1981).
[15] C. Chollet *et al.*, Phys. Lett. **127B**, 331 (1983).
[16] M. Anghinolfi *et al.*, Phys. Rev. C **47**, R922 (1993).
[17] N. Bianchi *et al.*, Phys. Lett. B **309**, 5 (1993).
[18] N. Bianchi *et al.*, Phys. Rev. C **48**, 1785 (1993).
[19] R. Vandenbosch and J. R. Huizenga, *Nuclear Fission* (Academic Press, New York, 1973).
[20] N. Bianchi *et al.*, Phys. Rev. C **54**, 1688 (1996).
[21] A. S. Iljinov, E. A. Cherepanov, and Y. F. Chigrinov, Sov. J. Nucl. Phys. **32**, 166 (1980).
[22] J. B. Martins *et al.*, Phys. Rev. C **44**, 354 (1991).
[23] C. Guaraldo *et al.*, Nuovo Cimento A **103**, 607 (1990).
[24] L. O. Dallin, in *Proceedings of the Particle Accelerator Conference*, edited by F. Bennett and J. Kopta (IEEE, Chicago, 1989), p. 22.
[25] J. M. Vogt *et al.*, Nucl. Instrum. Methods Phys. Res. A **234**, 198 (1993).
[26] G. Hempel, F. Hopkins, and G. Schatz, Nucl. Instrum. Methods **131**, 445 (1975).
[27] H. Stelzer, Nucl. Instrum. Methods **133**, 409 (1976).
[28] G. Gaukler *et al.*, Nucl. Instrum. Methods **141**, 115 (1977).
[29] A. Breskin and N. Zwang, Nucl. Instrum. Methods **144**, 609 (1977).
[30] Y. Eyal and H. Selzer, Nucl. Instrum. Methods **155**, 157 (1978).
[31] M. Just *et al.*, Nucl. Instrum. Methods **148**, 283 (1978).
[32] W. Gunter *et al.*, Nucl. Instrum. Methods **163**, 459 (1979).
[33] J. D. T. Arruda-Neto *et al.*, Nucl. Instrum. Methods Phys. Res. **190**, 203 (1981).
[34] J. C. Sanabria *et al.*, Nucl. Instrum. Methods (in press).
[35] J. C. Sanabria, Ph.D. thesis, The George Washington University, 1999.
[36] J. C. Sanabria *et al.* (unpublished).
[37] R. C. Carrasco and E. Oset, Nucl. Phys. **A536**, 445 (1992).
[38] K. Kikuchi and M. Kawai, *Nuclear Matter and Nuclear Reactions* (North-Holland, Amsterdam, 1968).